Defence Research and Development Canada
Recherche et développement pour la défense Canada

DEFENCE R&D DÉFENSE

Numerical recipes to determine the performance of multi-channel GMTI radars

Christoph H. Gierull

Defence R&D Canada – Ottawa

Technical Memorandum
DRDC Ottawa TM 2011-230
December 2011

Canada

Numerical recipes to determine the performance of multi-channel GMTI radars

Christoph H. Gierull
Defence R&D Canada – Ottawa

Defence R&D Canada – Ottawa
Technical Memorandum
DRDC Ottawa TM 2011-230
December 2011

Principal Author

Original signed by Christoph H. Gierull

Christoph H. Gierull

Approved by

Original signed by Anthony Damini

Anthony Damini
Acting Head/Radar Systems Section

Approved for release by

Original signed by Chris McMillan

Chris McMillan
Chair/Document Review Panel

Abstract

This memorandum presents a robust and relatively simple-to-implement numerical approach for computing figures of merits, such as probability of detection and probability of false alarms. Figures of merit can be computed to a chosen arbitrary accuracy for generic Ground Moving Target Indicator (GMTI) radars under specified general assumptions for the interfering clutter and desired target signal statistics. The approach expands the well-published single receiver channel analysis to multi-channel approaches, such as the Displaced Phase Center Antenna DPCA or Space-Time Adaptive Processing (STAP) without relying on a common approximation for non-homogeneous clutter (texturizing the noise) to make the models mathematically tractable. The derivation comprises a flexible modeling approach permitting solutions for a variety of target models including deterministic targets and the fluctuating target Radar Cross Section (RCS) Swerling target models. The approach additionally allows for the averaging of multiple independent measurements (multi-looking). The capability and usefulness of this new approach is demonstrated based on numerical examples with a variety of different radar parameter settings.

Résumé

Le présent document décrit une approche numérique robuste et assez simple à appliquer pour calculer les facteurs de mérite, comme la probabilité de détection et la probabilité de fausses alarmes. Les facteurs de mérite peuvent être calculés avec la précision arbitraire choisie pour des radars d'indication de cible terrestre mobile (ICTM) génériques en fonction de certaines hypothèses générales relatives au clutter brouilleur et aux statistiques sur les signaux des cibles souhaitées. L'approche élargie l'analyse bien documentée sur les canaux de récepteur simple aux approches multicanaux, comme l'antenne à centre de phase déplacé (DPCA) ou le traitement adaptatif espace temps (STAP), sans utiliser d'approximation commune pour le clutter non homogène (texturation du bruit) afin de permettre la résolution mathématique des modèles. La dérivation comporte une approche souple de modélisation qui permet des solutions pour divers modèles de cibles, y compris des cibles déterministes et des modèles de cibles de Swerling à surface équivalente radar (SER) fluctuante. Cette approche permet en outre de calculer la moyenne des mesures indépendantes multiples (multivisées). La capacité et l'utilité de cette nouvelle approche sont démontrées au moyen d'exemples numériques comportant divers réglages des paramètres radar.

This page intentionally left blank.

Executive summary

Numerical recipes to determine the performance of multi-channel GMTI radars

Christoph H. Gierull; DRDC Ottawa TM 2011-230; Defence R&D Canada – Ottawa; December 2011.

Background: Recently developed DND essential requirements for future space-based SAR missions, such as RADARSAT Next Generation (RNG), specify the inclusion of a Ground Moving Target Indication (GMTI) capability to overcome existing remote sensing deficiencies. The currently envisioned approach for the utilization of RADARSAT-2 (Polar Epsilon), and the upcoming RADARSAT Constellation Mission (RCM) (Polar Epsilon 2) as space-based surveillance platforms focuses on the operational monitoring of Canada's ocean approaches using single-channel SAR image based products. SAR image based ship detection has been proven to work sufficiently well under relatively calm weather conditions in the open ocean but suffers significant performance shortfalls in more challenging clutter environments, such as, high sea states, steep incidence angles, littoral zones or ice-infested waters like the Arctic. Under these circumstances the vessel's image signature cannot be easily discriminated from the similarly strong background returns. Over the last several years DRDC's Moving Object Detection EXperiment (MODEX) has theoretically and experimentally confirmed that sophisticated GMTI from space is indeed possible even for the most demanding terrain (including land application). By splitting RADARSAT-2's SAR antenna into two halves and recording the two channels separately, the ability to effectively suppress background interference through STAP was convincingly demonstrated. However, one crucial open question remained, namely, how to model and generalize these promising results so as to allow the calculation of objective measures of GMTI performance for future space-based systems which will likely possess different radar architectures and system parameters.

Principal results: This memorandum derives general and flexible mathematical tools to numerically compute the GMTI performance of generic multi-channel radar systems (airborne and space-based) for a wide range of statistical clutter and target models with an arbitrary high accuracy. In particular, the analysis comprises:

- different multi-channel GMTI processing techniques including the conventional sum channel (e.g. basic SAR image based detection), DPCA and the optimum Wiener filter (STAP),
- a compound statistical model for heterogeneous clutter with arbitrary probability distribution for the texture random variable, e.g. Gamma or inverse Gamma

distribution,

- a correct accounting for additive Gaussian receiver noise that, unlike the description in some classical literature, is truly not impacted by the texture e.g. the well-known and often used K-distribution for the sea surface,
- flexible target signal characteristics including constant RCS (Swerling 0) and all random Swerling I-IV RCS models,
- multi-looking to enhance detection performance, i.e. averaging of several independent samples including the realistic scenario that the target might occur only in L-out-of-n measurements.

Significance of results: The objective of this report is to introduce a theoretical framework which permits the assessment of GMTI performance from generic multi-channel SAR systems and allows comparison to conventional image-based techniques. The presented tools have already been used for a preliminary quality assessment of a potential GMTI mode on the soon-to-be-launched RCM, and have identified a large potential performance improvement. In addition they were also used during DND's requirement definition finding exercise for the Canadian Space Agency's (CSA) RADARSAT Next Generation study. The flexibility of the tools has been proven to be useful, as the statistical models can be modified whenever updated or new models (e.g. new ship RCS models) are available.

Future work: the results presented in this paper are based on a purely theoretical development and, as such, future work should be undertaken to evaluate and verify these results with real experimental multi-channel space-based SAR data recorded from such platforms as RADARSAT-2.

Sommaire

Numerical recipes to determine the performance of multi-channel GMTI radars

Christoph H. Gierull ; DRDC Ottawa TM 2011-230 ; R & D pour la défense Canada – Ottawa ; décembre 2011.

Introduction : Les besoins essentiels récemment développés du MDN pour les futures missions SAR à partir de l'espace, comme un RADARSAT de prochaine génération (RPG), précisent l'inclusion d'une capacité d'ICTM pour corriger les lacunes actuelles de détection à distance. L'approche actuellement envisagée pour l'utilisation de RADARSAT 2 (Polar Epsilon) et de la mission de la Constellation RADARSAT (MCR) [Polar Epsilon 2] à venir comme plates formes de surveillance à partir de l'espace est orientée sur la surveillance opérationnelle des approches océaniques du Canada au moyen de produits axés sur les images SAR monocanal. Il s'est avéré que la détection de navires fondée sur les images SAR fonctionne assez bien dans des conditions météorologiques relativement calmes en plein océan, mais ses performances sont très insuffisantes dans des environnements de clutter plus importants, dont une mer de force élevée, des angles d'incidence élevés, des zones littorales ou des eaux infestées de glace, comme dans l'Arctique. Dans ces circonstances, la signature de l'image du navire est difficile à discriminer des échos parasites forts et similaires. Au cours des dernières années, l'expérience de détection des objets mobiles (MODEX) de RDDC a permis de confirmer théoriquement et expérimentalement que l'ICTM perfectionné à partir de l'espace est en fait possible même sur les terrains les plus exigeants (y compris les applications terrestres). En divisant en deux l'antenne SAR de RADARSAT 2 et en enregistrant les deux canaux séparément, on a démontré de façon convaincante la capacité de supprimer efficacement le brouillage parasite au moyen du STAP. Il reste toutefois une question cruciale : comment doit on modéliser et généraliser ces résultats prometteurs pour permettre le calcul de mesures objectives du rendement de l'ICTM pour les systèmes spatiaux futurs, dont les architectures radar et les paramètres de système sont sans doute différents ?

Résultats principaux : Le présent document développe des outils mathématiques souples et généraux destinés au calcul numérique des performances d'ICTM des systèmes radar multicanaux génériques (aéroportés et spatiaux) pour une vaste gamme de clutters statistiques et de modèles de cibles avec une précision arbitraire élevée. L'analyse comporte notamment :

– différentes techniques de traitement d'ICTM multicanaux, y compris le canal somme ordinaire (comme la détection axée sur les images SAR de base), la DPCA et le filtre de Wiener optimal (STAP) ;

– un modèle statistique composé pour le clutter hétérogène et doté d'une distribution de probabilité arbitraire pour la variable aléatoire de texture, comme la distribution Gamma ou Gamma inverse ;

– une bonne comptabilisation du bruit gaussien additif du récepteur qui, contrairement à ce qui est décrit dans certains documents classiques, n'est pas du tout sensible à la texture, comme la K-distribution bien connue et souvent utilisée pour la surface de la mer ;

– des caractéristiques souples de signaux de cible, y compris une SER constante (Swerling 0) et tous les modèles SER Swerling I-IV aléatoires ;

– des multivisées pour améliorer les performances de détection, comme un calcul de la moyenne de plusieurs échantillons distincts, y compris le scénario réaliste que la cible pourrait apparaître dans les mesures seulement L fois sur n.

Portée des résultats : Le présent rapport vise à introduire un cadre théorique qui permet d'évaluer les performances d'ICTM de systèmes SAR multicanaux génériques et de comparer des techniques traditionnelles axées sur les images. Les outils présentés ont déjà été utilisés pour effectuer une évaluation préliminaire de la qualité d'un mode d'ICTM possible sur la MCR, qui sera bientôt lancée, et ont mis en évidence des améliorations possibles importantes des performances. Ces outils ont en outre été utilisés pendant l'exercice de définition des besoins du MDN pour l'étude de la prochaine génération de RADARSAT de l'Agence spatiale canadienne (ASC). La souplesse des outils s'est avérée utile, car les modèles statistiques peuvent être modifiés lorsque des modèles mis à jour ou de nouveaux modèles (comme de nouveaux modèles SER de navires) sont disponibles.

Recherches futures : Les résultats fournis dans le présent document reposent sur un développement purement théorique et, en conséquence, des recherches futures devraient être entreprises pour évaluer et vérifier ces résultats par rapport aux données expérimentales réelles du SAR spatial multicanal enregistrées à partir de plates formes comme RADARSAT 2.

Table of contents

List of figures

List of listings

List of tables

This page intentionally left blank.

1 Introduction

Recently developed DND essential requirements for future space-based SAR missions, such as RADARSAT Next Generation (RNG), specify the inclusion of a Ground Moving Target Indication (GMTI) capability to overcome existing remote sensing deficiencies. The currently envisioned approach for the utilization of RADARSAT-2 (Polar Epsilon), and the upcoming RADARSAT Constellation Mission (RCM) (Polar Epsilon 2) as space-based surveillance platforms focuses on the operational monitoring of Canada's ocean approaches using single-channel SAR image based products. SAR image based ship detection has been proven to work sufficiently well under relatively calm weather conditions in the open ocean but suffers significant performance shortfalls in more challenging clutter environments, such as, high sea states, steep incidence angles, littoral zones or ice-infested waters like the Arctic. Under these circumstances the vessel's image signature cannot be easily discriminated from the similarly strong background returns. Over the last several years DRDC's Moving Object Detection EXperiment (MODEX) has theoretically and experimentally confirmed that sophisticated GMTI from space is indeed possible even for the most demanding terrain (including land application). By splitting RADARSAT-2's SAR antenna into two halves and recording the two channels separately, the ability to effectively suppress background interference through STAP was convincingly demonstrated. However, one crucial open question remained, namely how to model and generalize these promising results so as to allow the calculation of objective measures of GMTI performance for future space-based systems which will likely possess different radar architectures and system parameters.

In this memorandum a classic GMTI detection test based on the incoherent summation of several independent data samples is used to distinguish a target from the interfering background and noise. To guarantee a Constant False Alarm Rate (CFAR) property in the Neyman-Pearson sense, the knowledge of the Probability Density Function (pdf) of the test statistics is essential. This pdf must be known for different assumed statistical characteristics of the target, interfering background clutter and varying receiver noise. Given the highly non-linear nature of the test, the desired analytical derivation of the pdf is exceedingly difficult if not impossible. However, since only the resulting figure of merits are generally of interest (e.g. the probability of detection for a given pre-set false alarm rate) rather than the pdf itself, common statistical workshop tools such as Bayes-rule can be utilized to yield solutions that can be comfortably evaluated by a computer.

In order to incorporate the more realistic heterogeneous nature of many clutter surfaces, for instance land or ice-infested water, a commonly accepted compound model will be adopted. This compound or product model utilizes the modification of the homogeneous clutter model by an independent texture random variable. It has been

shown, however, that an inherent approximation which is commonly used to derive the compound clutter model and makes it mathematical tractable (including the classic K-distribution for sea surface SAR data modeling [1]) is strictly speaking invalid, particularly for space-based radars. More specifically, for space-based systems the respective power levels, i.e., Signal-to-Noise Ratio (SNR) and Clutter-to-Noise Ratio (CNR), are significantly smaller than for airborne systems mainly due to the much larger standoff ranges. Thus, the implicit multiplication of the speckle and the noise with the texture random variable (RV) (dubbed texturizing of noise) that is commonly assumed is not justifiable anymore, e.g. [2]. The analysis in this memorandum takes this correctly into account. Further, it has been shown that a texture distribution based on the inverse chi-square (or inverse Gamma) model, which had been successfully applied on airborne data in the past, can also be used for the space-based analysis [3, 4], and hence is also considered in this report.

The theoretical concept of how to derive the detection probability in this memorandum is based on original work by Shnidman [5, 6, 7, 8]. See also [1] as well as [9].

2 Statistical models for the measured data

In this report we confine ourselves, without loss of generality, to a two-channel GMTI radar system, e.g. such as RADARSAT-2, for simplicity and clarity of notation. Let us assume that the data of the two channels are combined in vector form as

$$\boldsymbol{Z}_k = \begin{bmatrix} z_k(1) \\ z_k(2) \end{bmatrix}, \tag{1}$$

where k may represent one resolution cell in the spatial domain, for instance properly sub-sampled spatial pixels after SAR processing. In general, however, it could also denote the time domain (raw data) or the frequency domain (Doppler). In the following vectors are written in bold and italic while matrices are in bold but straight font. Transposition of a matrix is denoted by superscript $'$ and conjugate complex transpose by *, respectively.

A rather general statistical model for this kind of measured radar data reads

$$\boldsymbol{Z}_k = \boldsymbol{S}_k + \Delta \cdot \boldsymbol{C}_k + \boldsymbol{N}_k, \tag{2}$$

where the individual terms represent the following:

1. If deterministic, the target signal may be written as

$$\boldsymbol{S}_k := \boldsymbol{s} = \sigma_t \begin{bmatrix} e^{j\vartheta_1} \\ e^{j\vartheta_2} \end{bmatrix}. \tag{3}$$

While the common amplitude σ_t determines the related SNR, mainly driven by the target's RCS, the phase difference relates to the target's across-track velocity component v_y via

$$\vartheta_2 - \vartheta_1 \cong \frac{2\pi}{\lambda}\, d\, \frac{v_y}{v_a}, \tag{4}$$

where λ denotes the wavelength, v_a the platform or antenna velocity and d the distance between the two receiving antennas, e.g. [10].

If the target return is fluctuating, for instance due to the superposition of many individual scatterers on an extended target like a ship, it can be modeled as a random variable (RV), $\boldsymbol{S}_k$, for instance, following a complex normal distribution

$$\boldsymbol{S}_k \sim \mathcal{N}_2^{\mathbb{C}}\left(\boldsymbol{0}, \mathbf{R}_{\mathbf{S}}\right),$$

with covariance matrix

$$\mathbf{R}_{\boldsymbol{S}} = \sigma_t^2 \begin{bmatrix} 1 & \rho_t e^{-j(\vartheta_2-\vartheta_1)} \\ \rho_t e^{j(\vartheta_2-\vartheta_1)} & 1 \end{bmatrix}. \tag{5}$$

For simplicity it will be assumed from here onwards that the inter-channel correlation of the target $\rho_t = 1$ (again without loss of generality). It will be shown in section 5.2 that the above model permits inclusion of all standard Swerling target models [11].

2. As superposition of many independent scattering echoes within one resolution cell, the clutter $\boldsymbol{C}_k$ of homogeneous terrain is commonly modeled as complex normal

$$\boldsymbol{C}_k \sim \mathcal{N}_2^{\mathbb{C}}\left(\boldsymbol{0}, \mathbf{R}_{\boldsymbol{C}}\right),$$

with covariance matrix

$$\mathbf{R}_{\boldsymbol{C}} = \sigma_c^2 \begin{bmatrix} 1 & 1 \\ 1 & 1 \end{bmatrix}. \tag{6}$$

Identical to the target, full correlation between the channels has been assumed, i.e. the clutter is stationary and the two channels are already properly co-registered and balanced [12]. The corresponding clutter power is denoted as σ_c^2. If channel abberations are considered as for instance discussed in [2], the off diagonal elements will deviate from unity magnitude.

3. The variable Δ is the texture RV used to model heterogeneity of the clutter process. In practice, one almost always encounters limitations in the model of a stationary zero-mean Gaussian process in each channel. Although the stationary Gaussian model is still locally suitable, the process is not stationary when the background reflectivity (variance σ_c^2) changes from one sample to the next. While it is still valid to assume that the mean of the process is zero

and stationary, the variance must be modeled as globally non-stationary. For instance, the variance of the SAR data will be quite different for grassy terrain as compared to urban terrain. In a scene containing both types (and more) of terrain, a statistical description of the RV shall be included to validate the model. To this end, the introduction of a texture random variable $\Delta \in [0, \infty)$ leads to the so-called product or compound model. Generally, the theoretical distribution generated assuming homogeneous conditions predicts fewer high valued samples than are actually measured. The purpose of the random variable Δ therefore is to suitably elongate the theoretical probability distribution.

Many authors have studied appropriate statistical models for Δ, for instance compare [13, 3, 14, 15]. Choosing, for instance the square-root of the chi-square model (or Gamma model) with pdf

$$f_{\Delta}(\delta) = \frac{2(\nu)^{\nu}}{\Gamma(\nu)} \delta^{(2\nu-1)} \exp\left(-\nu\delta^2\right), \tag{7}$$

results in the well-known K-distribution for the clutter[1] often used to model the sea surface [1, 16]. In contrast, several papers dealing with GMTI for land targets have adopted the square-root of the inverse chi-square model (or inverse Gamma model), $\chi^{-1/2}$ [3, 14] with pdf given by

$$f_{\Delta}(\delta) = \frac{2(\nu-1)^{\nu}}{\Gamma(\nu)} \delta^{-(2\nu+1)} \exp\left(-\frac{\nu-1}{\delta^2}\right), \tag{8}$$

its central moments by

$$\mathsf{E}\,\Delta^r = (\nu-1)^{r/2}\ \frac{\Gamma(\nu - r/2)}{\Gamma(\nu)} \qquad \nu > \frac{r}{2}. \tag{9}$$

One convenient property all texture models have in common is the unity of its second moment $\mathsf{E}\,\Delta^2 = 1$ in order not to unintentionally change the total clutter power σ_c^2. The texture parameter ν describes the degree of heterogeneity, i.e. the larger ν the more homogenous the scene.

Since the texture RV is constant for all k it is inherently assumed that it is fully correlated throughout one multi-look cell (containing n single look resolution cells). However, it may change from one multi-look cell to the next [17]. The more complicated case of only partially correlated texture has recently gained some attention, e.g. [18], but is not considered in this report.

4. The additive thermal noise is modeled as statistically white complex normal distributed with equal power σ_n^2 between the channels, i.e.

$$\boldsymbol{N}_k \sim \mathcal{N}_2^{\mathbb{C}}\left(\boldsymbol{0}, \mathbf{R}_{\boldsymbol{N}}\right),$$

[1] This is only the case if the noise is neglected or the texture is wrongly applied to both the clutter and the noise $\Delta \cdot (\boldsymbol{C} + \boldsymbol{N})$.

with

$$\mathbf{R}_{\boldsymbol{N}} = \sigma_n^2 \mathbf{I}_2, \tag{10}$$

where $\mathbf{I}_m$ describes the identify matrix of dimension m.

Note, all RV are assumed to be mutually statistically independent from each other.

3 Test statistic

Let us assume we use data from a set of $k = 1, \ldots, n$ statistically independent samples to decide whether or not a moving target is present in the measured data. For historical reasons the parameter n is often called number of looks within the SAR community. Statistically independent clutter cells are averaged in order to reduce the clutter contamination and therefore enhance the achievable SNR.

Now let us suppose that the decision whether or not a moving target is present in the multi-channel data is based on a general class of detectors of the form:

$$\begin{aligned} \overline{T} &= \|\mathbf{Z}^* \boldsymbol{u}\|^2 = \boldsymbol{u}^* \mathbf{Z}\mathbf{Z}^* \boldsymbol{u} \\ &= \sum_{k=1}^{n} |\boldsymbol{u}^* \boldsymbol{Z}_k|^2 , \end{aligned} \tag{11}$$

where $\boldsymbol{u}$ is a constant vector with $\|\boldsymbol{u}\|^2 = 1$. This class, often called square law detectors, comprises important techniques such as the SNCR optimum detector and Displace Phase Center Antenna (DPCA) technique [19] and also the simple sum of the channels (representing the SAR image), for which:

$$\boldsymbol{u}_{\text{opt}} = \frac{\mathbf{R}^{-1/2}\boldsymbol{s}}{\sqrt{\boldsymbol{s}^* \mathbf{R}^{-1} \boldsymbol{s}}}, \tag{12}$$

$$\boldsymbol{u}_{\text{DPCA}} = \frac{1}{\sqrt{2}} \begin{bmatrix} 1 \\ -1 \end{bmatrix}, \tag{13}$$

$$\boldsymbol{u}_{\text{sum}} = \frac{1}{\sqrt{2}} \begin{bmatrix} 1 \\ 1 \end{bmatrix}, \tag{14}$$

with $\mathbf{R} = \mathbf{R}_{\boldsymbol{C}} + \mathbf{R}_{\boldsymbol{N}}$. Note that the optimum beamformer $\boldsymbol{u}_{\text{opt}}$ simplifies to the difference of the channel outputs, i.e. $\boldsymbol{u}_{\text{DPCA}}$, under certain conditions [19].

To be more general, the target may only be present in L out of the total n data samples. All n realizations of the model (2) can be combined into the data matrix $\mathbf{Z}$:

$$\begin{aligned} \mathbf{Z} &= [\boldsymbol{Z}_1, \boldsymbol{Z}_2, \ldots, \boldsymbol{Z}_n] \\ &= \left[\begin{array}{llll} S_1(1) + \Delta\, C_1(1) + N_1(1), & \ldots, & S_L(1) + \Delta\, C_L(1) + N_L(1), & \\ S_1(2) + \Delta\, C_1(2) + N_1(2), & \ldots, & S_L(2) + \Delta\, C_L(2) + N_L(2), & \\ & & \Delta\, C_{L+1}(1) + N_{L+1}(1), & \ldots, \quad \Delta\, C_n(1) + N_n(1) \\ & & \Delta\, C_{L+1}(2) + N_{L+1}(2), & \ldots, \quad \Delta\, C_n(2) + N_n(2) \end{array} \right]. \end{aligned} \tag{15}$$

Let us assume for the moment that a) the texture is constant, i.e not fluctuating with $\Delta = \delta$ and hence acts as a mere scaling of the clutter power, and b) that the target signal be a deterministic point target as in (3). Under these conditions and with the above assumptions 1) to 4), the n elements of the matrix product of $\boldsymbol{u}$ and the data matrix $\mathbf{Z}$ in (15):

$$\begin{aligned}\Big(\boldsymbol{u}^*(\mathbf{Z}\big|\Delta, \boldsymbol{S}_k)\Big)' &:= \Big(\boldsymbol{u}^*(\mathbf{Z}\big|\Delta = \delta, \boldsymbol{S}_k = \boldsymbol{s})\Big)' \\ &= \begin{bmatrix} \boldsymbol{u}^*(\boldsymbol{Z}_1\big|\Delta, \boldsymbol{S}_k) \\ \boldsymbol{u}^*(\boldsymbol{Z}_2\big|\Delta, \boldsymbol{S}_k) \\ \vdots \\ \boldsymbol{u}^*(\boldsymbol{Z}_n\big|\Delta, \boldsymbol{S}_k) \end{bmatrix}\end{aligned} \tag{16}$$

follows a multi-variate complex normal distribution with expectations

$$\mathsf{E}\, \boldsymbol{u}^*(\boldsymbol{Z}_k\big|\Delta, \boldsymbol{S}_k) = \begin{cases} \mathsf{E}\, \boldsymbol{u}^* \boldsymbol{S}_k = \boldsymbol{u}^* \boldsymbol{s} & \text{if } k \le L \\ 0 & \text{else} \end{cases}, \tag{17}$$

and variancess

$$\begin{aligned}\mathsf{E}\left[\boldsymbol{u}^*(\boldsymbol{Z}_k\big|\Delta, \boldsymbol{S}_k) - \mathsf{E}\, \boldsymbol{u}^*(\boldsymbol{Z}_k\big|\Delta, \boldsymbol{S}_k)\right] &\left[\boldsymbol{u}^*(\boldsymbol{Z}_k\big|\Delta, \boldsymbol{S}_k) - \mathsf{E}\, \boldsymbol{u}^*(\boldsymbol{Z}_k\big|\Delta, \boldsymbol{S}_k)\right]^* \\ &= \boldsymbol{u}^*\, \mathsf{E}\left(\delta \boldsymbol{C}_k + \boldsymbol{N}_k\right)\left(\delta \boldsymbol{C}_k + \boldsymbol{N}_k\right)^* \boldsymbol{u} \\ &= \boldsymbol{u}^* \left(\delta^2\, \mathsf{E}\, \boldsymbol{C}_k \boldsymbol{C}_k^* + \mathsf{E}\, \boldsymbol{N}_k \boldsymbol{N}_k^*\right) \boldsymbol{u} \\ &= \delta^2 \boldsymbol{u}^* \mathbf{R}_{\boldsymbol{C}} \boldsymbol{u} + \boldsymbol{u}^* \mathbf{R}_{\boldsymbol{N}} \boldsymbol{u}.\end{aligned} \tag{18}$$

i.e.

$$\Big(\boldsymbol{u}^*\left(\mathbf{Z}\big|\Delta, \boldsymbol{S}_k\right)\Big)' \sim \mathcal{N}_n^{\mathbb{C}}\left(\boldsymbol{u}^* \boldsymbol{s} \begin{bmatrix} \boldsymbol{1}_L \\ \boldsymbol{0}_{n-L} \end{bmatrix}, \left(\delta^2 \boldsymbol{u}^* \mathbf{R}_{\boldsymbol{C}} \boldsymbol{u} + \boldsymbol{u}^* \mathbf{R}_{\boldsymbol{N}} \boldsymbol{u}\right)\, \mathbf{I}_n\right), \tag{19}$$

where $\boldsymbol{0}_\nu$ and $\boldsymbol{1}_\nu$ are ν-dimensional vectors of zeros or ones, respectively. As a consequence of (19), the conditional test statistics in (11)

$$\Big(\overline{T}\big|\Delta, \boldsymbol{S}_k\Big) := \Big(\overline{T}\big|\Delta = \delta, \boldsymbol{S}_k = \boldsymbol{s}\Big) = \sum_{k=1}^{n} \left|\boldsymbol{u}^*(\boldsymbol{Z}_k\big|\Delta, \boldsymbol{S}_k)\right|^2 \tag{20}$$

as the sum of incoherently integrated independent complex normal distributed looks is non-central χ^2-distributed with pdf

$$f_{\overline{T}|\Delta, \boldsymbol{S}_k}(\bar{t}; \delta, \boldsymbol{s}) = \left(\frac{1}{\overline{\sigma}^2(\delta)}\right)^{\frac{n+1}{2}} \left(\frac{\bar{t}}{\overline{\omega}(\delta, \boldsymbol{s})}\right)^{\frac{n-1}{2}} \exp\left\{-\frac{\bar{t}}{\overline{\sigma}^2(\delta)}\right\}\, \mathrm{I}_{n-1}\left(2\sqrt{\frac{\overline{\omega}(\delta, \boldsymbol{s})}{\overline{\sigma}^2(\delta)}\bar{t}}\right), \tag{21}$$

with

$$\overline{\sigma}^2(\delta) = \boldsymbol{u}^* \left(\delta^2 \mathbf{R}_{\boldsymbol{C}} + \mathbf{R}_{\boldsymbol{N}}\right) \boldsymbol{u} \tag{22}$$

$$\overline{\omega}(\delta, \boldsymbol{s}) = \frac{\sum_{k=1}^{L} \boldsymbol{u}^* \boldsymbol{S}_k \boldsymbol{S}_k^* \boldsymbol{u}}{\overline{\sigma}^2(\delta)} = \frac{L\left|\boldsymbol{u}^* \boldsymbol{s}\right|^2}{\overline{\sigma}^2(\delta)} = \frac{a}{\overline{\sigma}^2(\delta)}, \tag{23}$$

where the signal contribution has been combined into the parameter $a = L\,|\boldsymbol{u}^*\boldsymbol{s}|^2$. The term $\mathrm{I}_m(\cdot)$ denotes the Bessel function of the first kind of order m. For simplicity of notation in the subsequent derivation, the dependency of $\overline{\sigma}$ and $\overline{\omega}$ on the variables δ and $\boldsymbol{s}$ will be omitted wherever doable without confusion.

It is convenient to normalize the test statistic such that the expectation of the test without the presence of a target is one. According to (11), the expectation of T can be expressed in case of clutter plus noise only as

$$\begin{aligned}
\mathsf{E}\,\overline{T} &= \mathsf{E}\,\boldsymbol{u}^* \sum_{k=1}^{n} (\Delta\,\boldsymbol{C}_k + \boldsymbol{N}_k)\,(\Delta\,\boldsymbol{C}_k + \boldsymbol{N}_k)^*\,\boldsymbol{u} \\
&= \cancel{(\mathsf{E}\,\Delta^2)^{-1}}\,\boldsymbol{u}^* \sum_{k=1}^{n} \mathsf{E}\,\boldsymbol{C}_k\boldsymbol{C}_k^*\boldsymbol{u} + \boldsymbol{u}^* \sum_{k=1}^{n} \mathsf{E}\,\boldsymbol{N}_k\boldsymbol{N}_k^*\boldsymbol{u} \\
&= n\,\boldsymbol{u}^*\,(\mathbf{R}_{\boldsymbol{C}} + \mathbf{R}_{\boldsymbol{N}})\,\boldsymbol{u} = n\sigma^2, \qquad (24)
\end{aligned}$$

where $\sigma^2 = \boldsymbol{u}^*\,(\mathbf{R}_{\boldsymbol{C}} + \mathbf{R}_{\boldsymbol{N}})\,\boldsymbol{u}$. Then, the pdf of the normalized conditional test

$$\Big(T\big|\Delta, \boldsymbol{S}_k\Big) = \frac{\Big(\overline{T}|\Delta, \boldsymbol{S}_k\Big)}{n\sigma^2}$$

can be computed via (21) as

$$f_{T|\Delta,\boldsymbol{S}_k}(t;\delta,\boldsymbol{s}) = n\sigma^2 f_{\overline{T}|\Delta,\boldsymbol{S}_k}(n\sigma^2 t;\delta,\boldsymbol{s})$$

or

$$f_{T|\Delta,\boldsymbol{S}_k}(t;\delta,\boldsymbol{s}) = \left(\frac{n\sigma^2}{\overline{\sigma}^2}\right)^{\frac{n+1}{2}} \left(\frac{t}{\overline{\omega}}\right)^{\frac{n-1}{2}} \exp\left\{-\frac{n\sigma^2}{\overline{\sigma}^2}t - \overline{\omega}\right\} \mathrm{I}_{n-1}\left(2\sqrt{\frac{n\sigma^2}{\overline{\sigma}^2}\overline{\omega}t}\right). \qquad (25)$$

Substituting $\overline{\omega} = a/\overline{\sigma}^2$ as in (23), (25) can be re-written as

$$\begin{aligned}
&f_{(T|\Delta,A)}(t;\delta,a) = \big(n\sigma^2\big)^{\frac{n+1}{2}}\,\frac{1}{\overline{\sigma}^2}\left(\frac{t}{a}\right)^{\frac{n-1}{2}} \exp\left\{-\frac{n\sigma^2 t + a}{\overline{\sigma}^2}\right\} \mathrm{I}_{n-1}\left(\frac{2}{\overline{\sigma}^2}\sqrt{n\sigma^2 a t}\right) \\
&\text{with} \\
&\qquad \sigma^2 = \boldsymbol{u}^*\,(\mathbf{R}_{\boldsymbol{C}} + \mathbf{R}_{\boldsymbol{N}})\,\boldsymbol{u} \\
&\qquad \overline{\sigma}^2 = \boldsymbol{u}^*\,\big(\delta^2\mathbf{R}_{\boldsymbol{C}} + \mathbf{R}_{\boldsymbol{N}}\big)\,\boldsymbol{u} \\
&\qquad a = L\,|\boldsymbol{u}^*\boldsymbol{s}|^2 = L\,\boldsymbol{u}^*\boldsymbol{s}\boldsymbol{s}^*\boldsymbol{u}.
\end{aligned} \qquad (26)$$

The actual test now has to decide if the Hypothesis $\mathfrak{H}$ or the Alternative $\mathfrak{A}$

$$\mathfrak{H}: \quad \sigma_t = 0 \quad \text{(interference alone)} \qquad (27)$$

$$\mathfrak{A}: \quad \sigma_t \neq 0 \quad \text{(interference plus target)} \qquad (28)$$

is valid based on n measurements $\boldsymbol{Z}_1, \ldots, \boldsymbol{Z}_n$ related to the model (2)

$$\boldsymbol{Z}_k = \boldsymbol{S}_k(\sigma_t) + \Delta \cdot \boldsymbol{C}_k + \boldsymbol{N}_k$$

when fed into the detector T in (11).

In the Neyman-Pearson sense, the optimum test is given by the probability ratio

$$\frac{f_{\mathfrak{H}}(T(\mathbf{Z}))}{f_{\mathfrak{A}}(T(\mathbf{Z}))} \gtrless \eta, \tag{29}$$

for which a decision "target" is made when the ratio between the probability density functions (pdf) of the test statistic (11) under the hypothesis and the alternative succeeds a threshold η.

This class of detectors must deal with two kinds of possible errors. The first kind occurs when the test decides on target (alternative $\mathfrak{A}$) albeit the hypothesis $\mathfrak{H}$ is true. Such a detection represents a false alarm and will occur with a certain false alarm probability P_{fa}. The second kind of error relates to the case that the detector does not respond although a target is present in the data, which represents a missed target. Its corresponding probability of missing is denoted as $P_{\mathrm{mi}} = 1 - P_{\mathrm{d}}$, where P_{d} is the complementary probability of detection.

These probabilities are depicted in Fig. 1. The red curve illustrates the test pdf under the hypothesis, while the black one shows the pdf under the alternative, i.e. that a target is present in the data. For a specified threshold η the P_{fa} is given a the area under the pdf along the tail from η outwards to infinity, Fig. 1(a). In practice, however, not the threshold is preset or a priori known but the maximally tolerable P_{fa}, for which the appropriate threshold needs to be determined. Once the threshold is known, the P_{d}, as the quality measure of the test, can be computed as the area under the pdf under the alternative, Fig. 1(b).

The main objective of the report is to identify reliable numerical ways to compute these values for the rather general statistical data model (2).

4 False alarm rate

As mentioned above, the appropriate detection threshold η for a chosen false alarm rate P_{fa} can be computed as the integral over the pdf

$$P_{\mathrm{fa}}(\eta) = \int_{\eta}^{\infty} f_T(t; \delta, a = 0)\, dt, \tag{30}$$

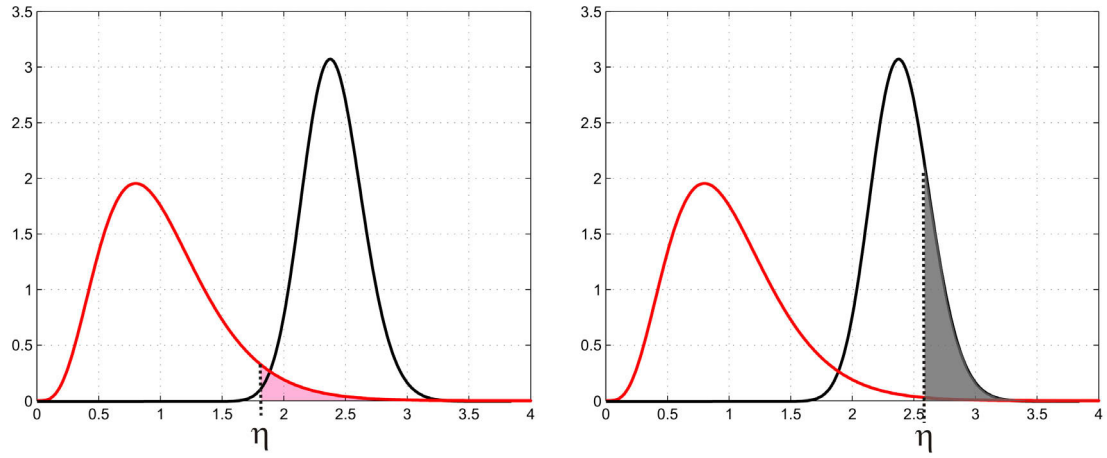

(a) P_{fa}. (b) P_{d}.

Figure 1: *Illustration of Probability of false alarm P_{fa} and detection P_{d}, respectively for two chosen thresholds η. The red curve represents a pdf under the hypothesis, i.e. clutter plus noise while the black curve represents a pdf under the alternative, i.e. the presence of a target in the interference.*

where the integral has to be evaluated when the signal is absent, i.e. for $a = 0$, see Fig. 1(a). The marginal pdf in (30) can be expressed using Bayes rule via integration over the conditional density function for a given texture:

$$f_T(t;\delta,0) = \int_0^\infty f_{T|\Delta=\delta}(t;\delta,a=0)\, f_\Delta(\delta)\, d\delta. \tag{31}$$

Inserting (31) into (30) and using the conditional density in (26) as well as the result in Annex (A.3) one gets

$$P_{\mathrm{fa}}(\eta) = \int_\eta^\infty \int_0^\infty \left(\frac{n\sigma^2}{\overline{\sigma}^2}\right)^n \frac{t^{n-1}}{\Gamma(n)} \exp\left\{-\frac{n\sigma^2}{\overline{\sigma}^2} t\right\} f_\Delta(\delta)\, d\delta\, dt. \tag{32}$$

Recalling that $\overline{\sigma}^2$ is a function of δ and after switching the order of integration yields

$$P_{\mathrm{fa}}(\eta) = \frac{1}{\Gamma(n)} \int_0^\infty \cancel{\left(\frac{n\sigma^2}{\overline{\sigma}^2(\delta)}\right)^n} \underbrace{\left(\int_\eta^\infty t^{n-1} \exp\left\{-\frac{n\sigma^2}{\overline{\sigma}^2(\delta)} t\right\} dt\right)}_{\frac{\Gamma\left(n, \frac{n\sigma^2}{\overline{\sigma}^2(\delta)}\right)}{\cancel{\left(\frac{n\sigma^2}{\overline{\sigma}^2(\delta)}\right)^n}}} f_\Delta(\delta)\, d\delta, \tag{33}$$

where the inner integral has been solved by using the result in ([20], 3.381-3). Finally the false alarm rate for heterogeneous compound clutter can be computed via:

$$\begin{aligned} P_{\text{fa}}(\eta) &= \frac{1}{\Gamma(n)} \mathsf{E}_{\Delta} \left\{ \Gamma\left(n, \frac{n\sigma^2}{\overline{\sigma}^2(\Delta)}\eta\right) \right\} \\ &= \frac{1}{\Gamma(n)} \int_0^{\infty} \Gamma\left(n, \frac{n\sigma^2}{\overline{\sigma}^2(\delta)}\eta\right) \, f_{\Delta}(\delta) \, d\delta, \end{aligned} \tag{34}$$

where E_X denotes the expectation with respect to the RV X. Note, the same result has already been presented, for instance, in [9, 21, 1]. For $\eta = 0$ we yield correctly $P_{\text{fa}}(0) = \cancel{\Gamma(n)}/\cancel{\Gamma(n)} = 1$ regardless of the chosen model for the texture.

The pdf for homogeneous clutter can be deduced from (34) as a special case, namely a constant, non-random, texture with $\Delta = \delta = 1$, for which we get the well-known result:

$$P_{\text{fa}}^{\text{hom}}(\eta) = \frac{\Gamma(n, n\eta)}{\Gamma(n)}. \tag{35}$$

One simple and robust way to find the appropriate threshold for a given P_{fa} is to evaluate the function (34) for a varying threshold and using an interpolator to get a more accurate value. The Listing 1 illustrates a possible implementation in Matlab:

```
nue = 7.35; %*** texture parameter
n   = 4;    %*** no of looks
%*** Chose texture pdf
switch texture
    case 'GAMMA',           %*** square-root gamma
        texture_pdf = (@(x) 2*nue.^(nue)./gamma(nue)*x...
              .^(2*nue-1).*exp(-nue.*x.^2));
    case 'INVERSE GAMMA',   %*** %*** inverse square-root ...
          gamma
        texture_pdf = (@(x) 2*(nue-1).^(nue)./gamma(nue)*x...
              .^(-2*nue-1).*exp(-(nue-1)./x.^2));
end

%*** Compute power parameter
alph    = u'*Rc*u;
bet     = u'*Rn*u;
sigma2  = alph + bet;
```

```
%*** Compute Pfa
Keta      = 200;
eta       = linspace(0,15,Keta);
Pfa       = zeros(Keta,1);
errbnd    = zeros(Keta,1);
for keta = 1:Keta
    kernel = (@(x)gammainc(n*sigma2*eta(keta)./(alph*x.^2+...
          bet),n,'upper').*texture_pdf(x));
    [Pfa(keta),errbnd(keta)] = quadgk(kernel,0,inf,'RelTol...
          ',1e-8,'AbsTol',1e-12);
end
```

Listing 1: *Matlab Kernel to compute* P_{fa}.

5 Probability of detection

As stated in the introduction, two types of targets are considered within this report; a) an idealistic target signal with constant RCS and b) a more realistic fluctuating/random target RCS.

5.1 Deterministic target signal

A constant RCS in our context is modeled as a non-random signal amplitude a in the density function (26). As a first step, homogeneous clutter is considered such that also δ^2 is constant and non-random. Then, according to Fig. 1(b), the probability of detection P_{d} for a pre-determined threshold, given a suitable P_{fa}, can be calculated via the integral

$$(P_{\text{d}}|\Delta=\delta)^{\text{hom}}(\eta)=\int_{\eta}^{\infty} f_{T|\Delta}(t;\delta,a)\,dt. \tag{36}$$

Using the power series representation for the Bessel function

$$\mathrm{I}_{n-1}\left(\frac{2}{\overline{\sigma}^2}\sqrt{na\sigma^2 t}\right)=\sum_{\mu=0}^{\infty}\frac{1}{\Gamma(\mu+1)\Gamma(n+\mu)}\left(\frac{\sqrt{na\sigma^2 t}}{\overline{\sigma}^2}\right)^{n-1+2\mu} \tag{37}$$

in (26) and insert the result into (36) yields

$$
\begin{aligned}
(P_{\mathrm{d}}|\Delta=\delta)^{\mathrm{hom}}(\eta) &= \int_{\eta}^{\infty} \left(\frac{n\sigma^2}{\overline{\sigma}^2}\right)^{\frac{n+1}{2}} \left(\frac{t}{\cancel{a}}\right)^{\frac{n-1}{2}} e^{-\frac{n\sigma^2 t+a}{\overline{\sigma}^2}} \left(\frac{n\cancel{a}\sigma^2 t}{\overline{\sigma}^2}\right)^{\frac{n-1}{2}} \\
&\qquad \times \sum_{\mu=0}^{\infty} \frac{(na\sigma^2 t)^{\mu}}{\overline{\sigma}^{4\mu}\Gamma(\mu+1)\Gamma(n+\mu)}\, dt \\
&= \cancel{\left(\frac{n\sigma^2}{\overline{\sigma}^2}\right)^{n}} e^{-\frac{a}{\overline{\sigma}^2}} \sum_{\mu=0}^{\infty} \frac{(\cancel{n}a\cancel{\sigma^2})^{\mu}}{\overline{\sigma}^{\cancel{4}2\mu}\Gamma(\mu+1)\Gamma(n+\mu)} \underbrace{\int_{\eta}^{\infty} t^{n-1+\mu} e^{-\frac{n\sigma^2}{\overline{\sigma}^2}t}\, dt}_{\frac{\Gamma\left(n+\mu,\,\frac{n\sigma^2}{\overline{\sigma}^2}\eta\right)}{\cancel{\left(\frac{n\sigma^2}{\overline{\sigma}^2}\right)^{n}}\left(\frac{\cancel{n}\sigma^2}{\overline{\sigma}^2}\right)^{\mu}}}
\end{aligned}
\tag{38}
$$

and hence

$$
\boxed{(P_{\mathrm{d}}|\Delta=\delta)^{\mathrm{hom}}(\eta) = \exp\left\{-\frac{a}{\overline{\sigma}^2}\right\} \sum_{\mu=0}^{\infty} \left(\frac{a}{\overline{\sigma}^2}\right)^{\mu} \frac{\Gamma\left(n+\mu,\,\frac{n\sigma^2}{\overline{\sigma}^2}\eta\right)}{\Gamma(\mu+1)\Gamma(n+\mu)}.} \tag{39}
$$

As for a sanity check, let us consider two special cases: a) $\eta = 0$, for which (39) becomes correctly

$$
(P_{\mathrm{d}}|\Delta=\delta)^{\mathrm{hom}}(0) = \exp\left\{-\frac{a}{\overline{\sigma}^2}\right\} \underbrace{\sum_{\mu=0}^{\infty} \frac{1}{\Gamma(\mu+1)} \left(\frac{a}{\overline{\sigma}^2}\right)^{\mu}}_{\exp\left\{\frac{a}{\overline{\sigma}^2}\right\}} = 1,
$$

since $\Gamma(n+\mu,0) = \Gamma(n+\mu)$, and b) $\eta \to \infty$, for which qualitatively $\Gamma(n+\mu,\infty) = 0$ and hence correctly $(P_{\mathrm{d}}|\Delta=\delta)^{\mathrm{hom}}(\infty) = 0$.

For heterogeneous clutter, where the texture is not considered constant but a RV, the probability of detection can be derived via averaging (39) over the pdf of Δ:

$$
P_{\mathrm{d}}^{\mathrm{het}}(\eta) = \mathsf{E}_{\Delta}\left\{(P_{\mathrm{d}}|\Delta=\delta)^{\mathrm{hom}}(\eta)\right\} = \int_{0}^{\infty} (P_{\mathrm{d}}|\Delta=\delta)^{\mathrm{hom}}(\eta)\; f_{\Delta}(\delta)\, d\delta, \tag{40}
$$

which may be rewritten as

$$P_{\mathrm{d}}(\eta) = \sum_{\mu=0}^{\infty} \frac{a^{\mu}}{\Gamma(\mu+1)\Gamma(n+\mu)} \mathsf{E}_{\Delta} \left\{ \frac{\Gamma\left(n+\mu, \frac{n\sigma^2}{\overline{\sigma}^2(\Delta)}\eta\right)}{\overline{\sigma}^{2\mu}(\Delta)} \exp\left\{ -\frac{a}{\overline{\sigma}^2(\Delta)} \right\} \right\}. \quad (41)$$

where the superscript "het" has been omitted for clarity of notation.

The Listing 2 illustrates the basic implementation of (41) in Matlab:

```
alph     = real(u'*Rc*u);
bet      = real(u'*Rn*u);
sigma2   = alph + bet;
%
muevec   = sqrt(sigmat_2)*[1; exp(j*ATIphase)]; %*** target...
       vector
apara    = L*abs(u'*muevec)^2;                  %*** target...
       parameter used in pdfs
%
%*** TEXTURE
switch texture
    case 'GAMMA',           %*** square-root gamma
        texture_pdf = (@(x) 2*nue.^(nue)./gamma(nue)*x...
              .^(2*nue-1).*exp(-nue.*x.^2));
    case 'INVERSE GAMMA',   %*** inverse square-root gamma
        texture_pdf = (@(x) 2*(nue-1).^(nue)./gamma(nue)*x...
              .^(-2*nue-1).*exp(-(nue-1)./x.^2));
end
%
%*** Compute Pd for varying eta as function of Pfa
%***
PdArray  = zeros(Keta,1);
PdErrBnd = zeros(Keta,1);
for keta = 1:Keta
    if mod(keta,25) == 0
       keta
    end
    eta       = etaArray(keta);
    deltaSum  = 1; summe = 0; k = 0; kmax = 500;
    meanDelta = zeros(kmax+1,1);
    errbnd    = zeros(kmax+1,1);
    while deltaSum>1.0e-22 && k<kmax,
        kernel   = (@(x)gammainc(n*sigma2*eta./(alph*x.^2+...
```

```
            bet),n+k,'upper')./((alph*x.^2+bet).^k).*exp...
            (-apara./(alph*x.^2+bet)).*texture_pdf(x));
        [meanDelta(k+1),errbnd(k+1)] = quadgk(kernel,0,inf...
            ,'RelTol',1e-8,'AbsTol',1e-12);
        deltaSum = exp(k*log(apara)-gammaln(k+1))*...
            meanDelta(k+1); %*** 1/gamma(n+k) removed ...
            due to def. of gamminc
        summe    = summe + deltaSum;
        k = k+1;
    end
    if k==kmax
        warning(['Result may be inaccurate: deltaSum = ',...
            num2str(deltaSum)])
    end
    PdArray(keta)  = summe;
    PdErrBnd(keta) = deltaSum;
end
```

Listing 2: *Matlab Kernel to compute P_{d} for a constant target model.*

5.2 Random target signal

The description of different target models below is mostly borrowed from the excellent paper [5]. Most commonly used models for target reflection fluctuations are based on the Gamma (or χ^2) pdf. The nonfluctuating model (sometimes also called Swerling 0) in section 5.1 is unrealistic except for simple symmetric target shapes, such as spheres or dihedral and trihedral corner reflectors. In most cases the radar target is a complex extended object, which produces a wide variety of reflections as for instance a vessel or an aircraft.

The arguably most widely used models were introduced by Swerling [11]. The so-called Swerling I model assumes that all random target signals $\boldsymbol{S}_k$ for $k = 1, \ldots, L$ present in L out of the n single-look cell data are fully correlated but may vary from one multi-look cell to the next. Under assumption 1. listed in section 2 that $\boldsymbol{S}_k \sim \mathcal{N}_2^{\mathbb{C}}(\boldsymbol{0}, \mathbf{R_S})$, the target contribution in (23)

$$A = \sum_{k=1}^{L} \boldsymbol{u}^* \boldsymbol{S}_k \boldsymbol{S}_k^* \boldsymbol{u} = L \underbrace{\boldsymbol{u}^* \boldsymbol{S}_1 \boldsymbol{S}_1^* \boldsymbol{u}}_{\sim \Gamma_2 - \text{distr.}} \tag{42}$$

is Γ_2-distributed with 2 degrees of freedom (because of the real and imaginary parts). In contrast, for the Swerling II model it is assumed that the individual single-look

contributions are mutually statistically independent so that the sum in (42) is Γ_{2L}-distributed with $2L$ degrees of freedom. These two models can reasonably represent a large number of targets. Both models inherently assume that the individual single-look returns $\boldsymbol{S}_k$ are made up of a large number of independent similarly distributed scattering centers whose combined response is Gaussian distributed according to the Central Limit Theorem.

By adopting the generic Gamma distribution for A in (42) with pdf

$$f_A(a) = \frac{1}{\Gamma(M)\left(\frac{L}{M}\boldsymbol{u}^*\mathbf{R}_{\boldsymbol{S}}\boldsymbol{u}\right)^M}\, a^{M-1}\, \exp\left\{-\frac{a}{\frac{L}{M}\boldsymbol{u}^*\mathbf{R}_{\boldsymbol{S}}\boldsymbol{u}}\right\}, \tag{43}$$

all of the above models can be expressed through variation of the sole shape parameter M:

Swerling 0: $M = \infty$

Swerling I: $M = 1$

Swerling II: $M = L$

Swerling III: $M = 2$

Swerling IV: $M = 2L$

The less used Swerling models III and IV are minor variants of the first two models with Γ_4 and Γ_{4L} distributions [11], respectively and are not further considered in this report. Note, in all cases the expectation of A is

$$\begin{aligned} \mathsf{E}\, A &= \int_0^\infty a\, f_A(a)\, da = \frac{1}{\Gamma(M)\cancel{\left(\frac{L}{M}\boldsymbol{u}^*\mathbf{R}_{\boldsymbol{S}}\boldsymbol{u}\right)^M}} \underbrace{\int_0^\infty a^M e^{\frac{a}{\frac{L}{M}\boldsymbol{u}^*\mathbf{R}_{\boldsymbol{S}}\boldsymbol{u}}}\, da}_{\Gamma(M+1)\cancel{\left(\frac{L}{M}\boldsymbol{u}^*\mathbf{R}_{\boldsymbol{S}}\boldsymbol{u}\right)^{M+1}}} \\ &= L\,\boldsymbol{u}^*\mathbf{R}_{\boldsymbol{S}}\boldsymbol{u} = L\,\boldsymbol{u}^*\boldsymbol{s}\boldsymbol{s}^*\boldsymbol{u} = L\,|\boldsymbol{u}^*\boldsymbol{s}|^2 \stackrel{!}{=} a, \end{aligned} \tag{44}$$

as in (23).

To derive the pdf for textured clutter and fluctuating target reflection, we can treat (39) as a conditional P_d for given $A = a$ and integrate over both RVs, i.e.

$$P_\mathrm{d}(\eta) = \int_0^\infty \int_0^\infty (P_\mathrm{d}|\Delta = \delta, A = a)(\eta)\;\; f_A(a)\, f_\Delta(\delta)\;\; da\, d\delta, \tag{45}$$

where again the superscript "hom" has been omitted for notational clarity. Inserting (39) into (45) and focussing only on the inner integral for a moment we get

$$(P_{\mathrm{d}}|\Delta=\delta)(\eta) = \frac{1}{\Gamma(M)\,(\frac{L}{M}\boldsymbol{u}^{*}\mathbf{R}_{\boldsymbol{S}}\boldsymbol{u})^{M}} \sum_{\mu=0}^{\infty} \frac{\Gamma\left(n+\mu, \frac{n\sigma^2}{\overline{\sigma}^2(\delta)}\eta\right)}{\Gamma(\mu+1)\Gamma(n+\mu)\,\overline{\sigma}^{2\mu}(\delta)} \times \underbrace{\int_0^{\infty} a^{\mu+M-1} \exp\left\{-\left(\frac{1}{\overline{\sigma}^2(\delta)} + \frac{1}{\frac{L}{M}\boldsymbol{u}^{*}\mathbf{R}_{\boldsymbol{S}}\boldsymbol{u}}\right) a\right\} da}_{\Gamma(\mu+M)\left(\frac{1}{\overline{\sigma}^2(\delta)}+\frac{1}{\frac{L}{M}\boldsymbol{u}^{*}\mathbf{R}_{\boldsymbol{S}}\boldsymbol{u}}\right)^{-(\mu+M)}} \tag{46}$$

and after substituting $\xi = \frac{L}{M}\boldsymbol{u}^{*}\mathbf{R}_{\boldsymbol{S}}\boldsymbol{u}$ can be rewritten as

$$(P_{\mathrm{d}}|\Delta=\delta)(\eta) = \sum_{\mu=0}^{\infty} \frac{\Gamma(\mu+M)\Gamma\left(n+\mu, \frac{n\sigma^2}{\overline{\sigma}^2(\delta)}\eta\right)}{\Gamma(M)\Gamma(\mu+1)\Gamma(n+\mu)} \frac{\left(\frac{\xi}{\overline{\sigma}^2(\delta)}\right)^{\mu}}{\left(1+\frac{\xi}{\overline{\sigma}^2(\delta)}\right)^{\mu+M}}, \tag{47}$$

where the quotient in (47)

$$\frac{\xi}{\overline{\sigma}^2(\delta)} = \frac{\frac{L}{M}\boldsymbol{u}^{*}\mathbf{R}_{\boldsymbol{S}}\boldsymbol{u}}{\delta^2\boldsymbol{u}^{*}\mathbf{R}_{\boldsymbol{C}}\boldsymbol{u} + \boldsymbol{u}^{*}\mathbf{R}_{\boldsymbol{N}}\boldsymbol{u}} \tag{48}$$

represents the total Signal-to-Clutter-plus-Noise ratio SCNR(δ). According to (31) the final detection probability can be computed via

$$P_{\mathrm{d}}(\eta) = \sum_{\mu=0}^{\infty} \frac{\Gamma(\mu+M)}{\Gamma(M)\Gamma(\mu+1)\Gamma(n+\mu)}\ \mathsf{E}_{\Delta}\left\{\frac{\Gamma\left(n+\mu, \frac{n\sigma^2}{\overline{\sigma}^2(\Delta)}\eta\right)\left(\frac{\xi}{\overline{\sigma}^2(\Delta)}\right)^{\mu}}{\left(1+\frac{\xi}{\overline{\sigma}^2(\Delta)}\right)^{\mu+M}}\right\}. \tag{49}$$

Please note, it may be advantageous from a numerical point of view to replace the expectation in (49) with

$$\mathsf{E}_{\Delta}\left\{\frac{\Gamma\left(n+\mu, \frac{n\sigma^2}{\overline{\sigma}^2(\Delta)}\eta\right)\left(\frac{\overline{\sigma}^2(\Delta)}{\xi}\right)^{M}}{\left(1+\frac{\overline{\sigma}^2(\Delta)}{\xi}\right)^{\mu+M}}\right\} \tag{50}$$

as the power in the numerator of (50) is not going to infinity.

Again, the Listing 3 illustrates a possible implementation in Matlab:

```
switch texture
    case 'GAMMA',           %*** square-root gamma
        texture_pdf = (@(x) 2*nue.^(nue)./gamma(nue)*x...
              .^(2*nue-1).*exp(-nue.*x.^2));
    case 'INVERSE GAMMA',   %*** inverse square-root gamma
        texture_pdf = (@(x) 2*(nue-1).^(nue)./gamma(nue)*x...
              .^(-2*nue-1).*exp(-(nue-1)./x.^2));
    otherwise,
        error('texture pdf not supported yet')
end
switch target
    case 'SWERLING_{I}',
        s = 1;              %*** shape parameter for the ...
              pdf
    case 'SWERLING_{II}',
        s = L;
    otherwise,
        error('target pdf not supported yet')
end
sigma2 = uRcu + uRnu;

deltaSum  = 1; summe = 0; k = 0; kmax = 1000;
meanDelta = zeros(kmax+1,1);
errbnd    = zeros(kmax+1,1);
while deltaSum>1.0e-20 && k<kmax,
    kernel = (@(x)gammainc(n*sigma2*eta./(uRcu*x.^2+uRnu),...
          n+k,'upper').*(((uRcu*x.^2+uRnu)/uRtu).^s)./(1+ ...
          (uRcu*x.^2+uRnu)/uRtu).^(k+s).*texture_pdf(x));
    [meanDelta(k+1),errbnd(k+1)] = quadgk(kernel,0,inf,'...
          RelTol',1e-8,'AbsTol',1e-12);
    deltaSum = exp(gammaln(k+s)-gammaln(k+1)-gammaln(s))*...
          meanDelta(k+1); %*** 1/gamma(n+k) removed due to...
           def of gamminc
    summe  = summe + deltaSum;
    k = k+1;
end
if k==kmax
    warning(['Result may be inaccurate: deltaSum = ',...
          num2str(deltaSum)])
end
Pd  = summe;
Err = deltaSum;
```

Listing 3: *Matlab Kernel to compute P_d for a fluctuating target model.*

6 Numerical examples

This chapter presents several examples of the numerically evaluated P_{d} for different statistical clutter and target models and varying parameter settings. The main system parameters are chosen to correspond to those of RADARSAT-2. Relevant parameters that are used in the analysis and are common to all computations are listed in Table 1. According to (4), the corresponding target (ATI) phase equals 1.01 rad or 57.87°.

System parameter	Value
Wavelength λ	0.0555 m
Nr. of parallel receive channels M	2
Phase center separation $d/2$	3.75 m
Orbit height H	798.178 km
Satellite Velocity v_a	7000 m/s
Incidence angle at near range θ_n	45°
Target across-track ground velocity y_y	12 m/s
Noise power level σ_n^2	0 dB

Table 1: *System parameters of RADARSAT-2.*

The clutter covariance matrix was chosen to include aberrations c.f. (6):

$$\mathbf{R}_{\boldsymbol{C}} = \sigma_c^2 \begin{bmatrix} 1 & 0.99\exp\{j0.01\} \\ 0.99\exp\{-j0.01\} & 1, \end{bmatrix} \tag{51}$$

where the off-diagonal phase corresponds to slow motion of the background clutter of 10 cm/s. The target and clutter powers are chosen according to desired SNR and CNR values in dB to $\sigma_t^2 = 10^{\mathrm{SNR}/10}$ and $\sigma_c^2 = 10^{\mathrm{CNR}/10}$, respectively.

The first two examples compare the impact of different clutter texture models on the P_{d} for a Swerling 0 target model (constant RCS). Fig. 2 presents the Receiver Operating Characteristics (ROC), i.e. P_{d} (as in (41) & Listing 2) versus varying P_{fa} (as in (34) & Listing 1) for all three processing filters OPT (12), DPCA (13) and SUM (14). Fig. 2(a) presents the results for Gamma-distributed texture RV as in (7), Fig. 2(b) are the results for inverse Gamma-distributed texture RV (8). The number of looks was chosen as $n = 4$ with the target present in all looks, i.e. $L = 4$. The texture parameter was set to $\nu = 5$ to represent a moderately heterogeneous terrain and the power levels are fixed at SNR$=$ 10 dB and CNR $=$ 0 dB. As expected, the sum-channel without clutter suppression in Fig. 2(a) (e.g. the SAR image) (green) exhibits the worst detection performance followed by the DPCA (blue). The best performance is observed for the SCNR-optimum filter (red). Fig. 2(b) shows the corresponding curves for the same parameter settings as in Fig. 2(a) but with a different texture model. The first noteworthy observation is that the curves for DPCA are identical.

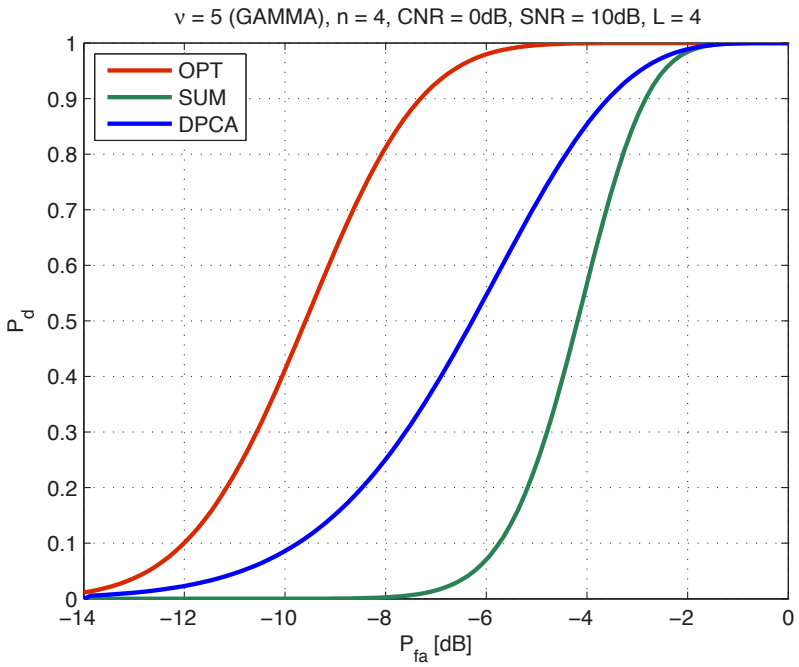

(a) Gamma-distributed texture.

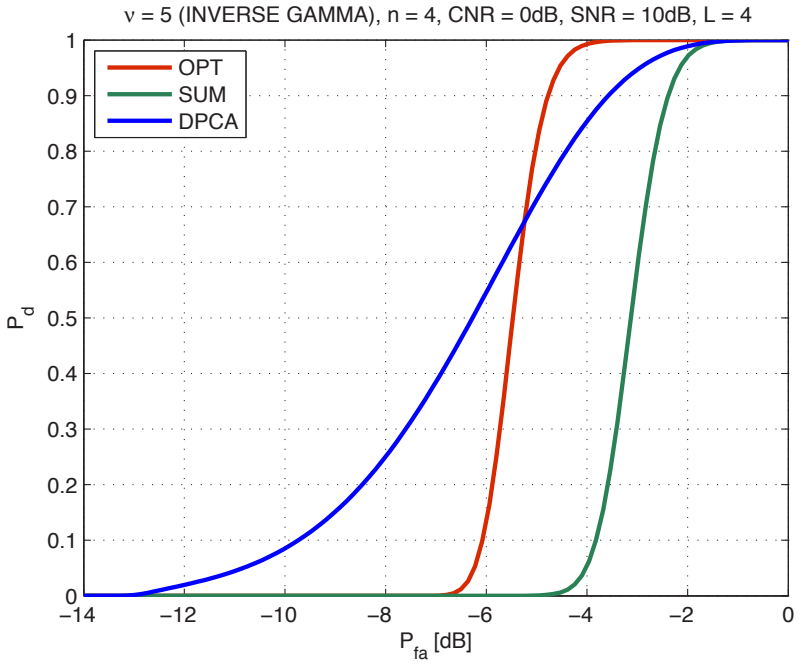

(b) Inverse Gamma-distributed texture.

Figure 2: *P_{d} versus P_{fa} for the different texture models and the Swerling 0 target model.*

This is expected as the subtraction of the two co-registered channels eliminates the influence of the texture RV Δ altogether. In contrast to the optimum processor, which applies the inverse of the covariance matrix to the data, does not properly cancel the effect of the texture on the data. Secondly, it is interesting to note that for the inverse Gamma case the blue and red curves intersect. In other words, for very low P_{fa}s, the DPCA method leads to a higher chance of detecting a moving target than the "optimum" processor. While this seems counterintuitive on first view, it is nevertheless correct and understandable as follows. The inverse Gamma pdf possesses a much more pronounced tail (higher probability of large spikes in the data), which pushes the detection threshold far out particularly for very low P_{fa}s. These large thresholds negatively impact the P_{d} as discussed in section 3, cf. Fig. 1(a) and Fig. 1(b). Although this finding makes the term "optimum processing" at least disputable for particular texture models, the red curve is generally steeper and hence reaches the larger P_{d} values before the blue DPCA curve. Since a relatively large P_{d}, such as $P_{\text{d}} = 90\%$ is often chosen as the required operating point for practical applications, e.g. [22], the Wiener filter can still be considered the superior choice in most cases.

Fig. 3 presents the ROC for the Swerling I target fluctuations for slightly different parameter settings than Fig. 2(a): $\nu = 7$, $n = L = 3$, CNR = 4.8 dB, SNR = 13 dB. As anticipated, the performance of all three models is significantly worse due to a combination of the fluctuating target RCS, the slightly lower number of looks and the increased clutter power.

Fig. 4 shows the comparison of the different target models for inverse Gamma texture model with $\nu = 11$ (slightly heterogeneous terrain), $n = L = 4$, CNR = 10 dB, SNR = 10 dB. As anticipated, the constant target RCS yields the best performance while the Swerling I case is significantly worse.

Fig. 5 illustrates the performance gain over increasing SNR for a Swerling 0 target for single-look data $n = L = 1$ with a CNR = 7.8 dB and moderately heterogeneous texture $\nu = 6$ following the inverse Gamma model. In this case a 20 dB target can be detected with 90% probability even for a very low false alarm rate of $P_{\text{fa}} = 10^{-12}$.

Similarly, Fig. 6 demonstrates the dependence of detection performance on an increasing value of ν for inverse Gamma distributed texture and the optimum processing filter. A Swerling II random target model with SNR = 10 dB has been selected with $n = L = 4$ looks, and a clutter power level of CNR = 0 dB. An increasing value of ν represents an increasingly homogenous background clutter. The observed performance in the most heterogeneous clutter $\nu = 2$ is considerably worse than that observed for larger values of ν. For texture parameters larger than 20 the ROC's approach quickly that of fully homogeneous clutter $\nu \to \infty$.

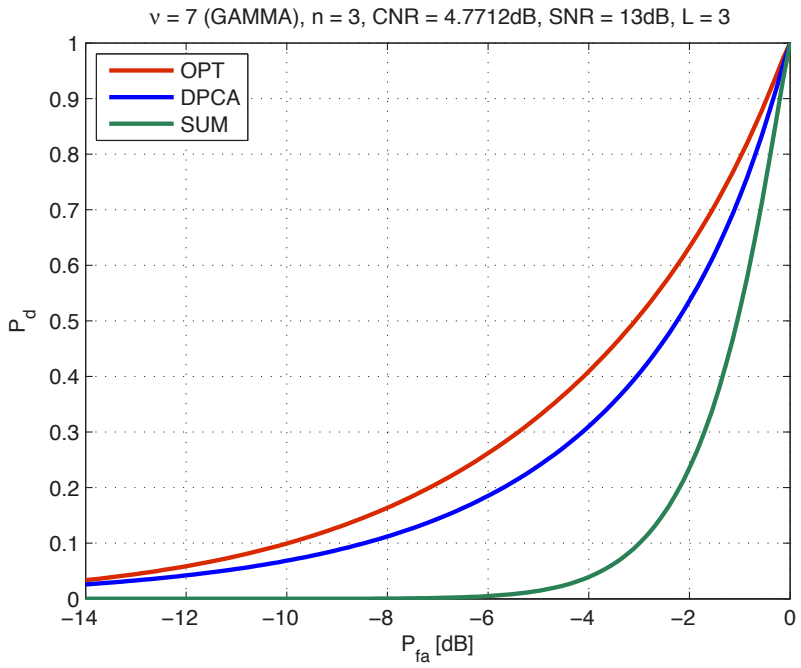

Figure 3: *P_{d} versus P_{fa} for the Gamma texture and Swerling I target models.*

Finally, Fig. 7 illustrates the performance gain of multi-looking independent samples in the sum channel. The chosen scenario comprises slightly heterogeneous $\nu = 11$ Gamma-distributed texture with a CNR of 0 dB. A Swerling II target was chosen with power level SNR = 10 dB. The solid curves in the figure represent the case for which the target is present in all looks ranging from $n = 1$ to $n = 9$. The results confirm a significant achievable improvement is obtained when the clutter can be smoothed by averaging. In contrast, a target covering only a portion of the multi-look data, e.g. $L = 3$ out of $n = 6$ cells is plotted as the dashed curve. It shows a considerable drop compared to the $n = L = 6$ case but still indicates that some improvement is obtained in comparison with simple single-looking.

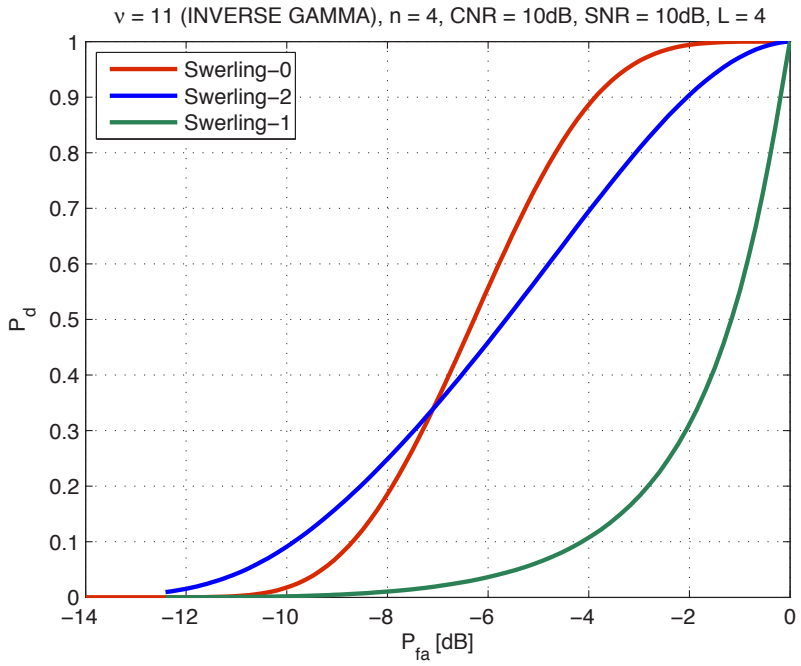

Figure 4: *P_{d} versus P_{fa} for the inverse Gamma texture and all three Swerling target models.*

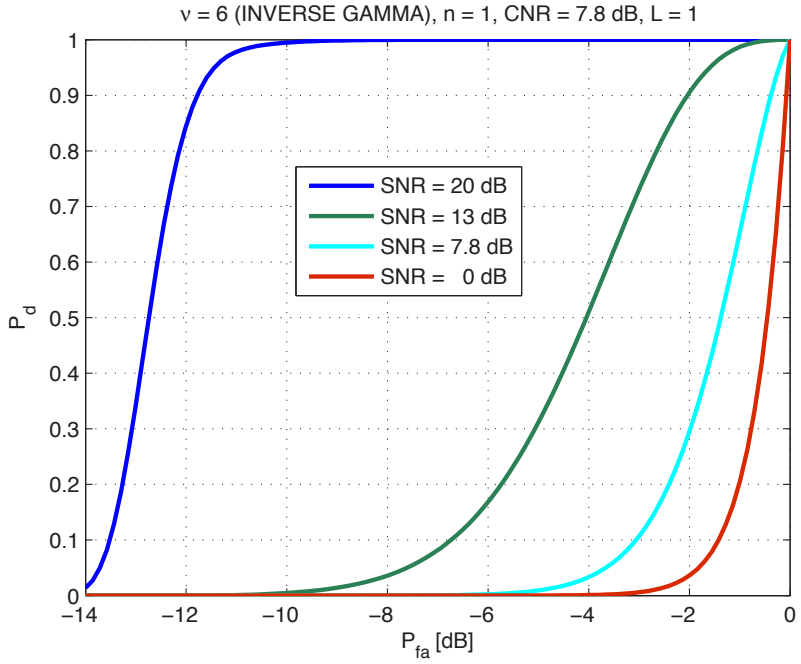

Figure 5: *P_{d} versus P_{fa} for the inverse Gamma texture and Swerling 0 target model with varying SNR. $n = 1$, $\nu = 6$.*

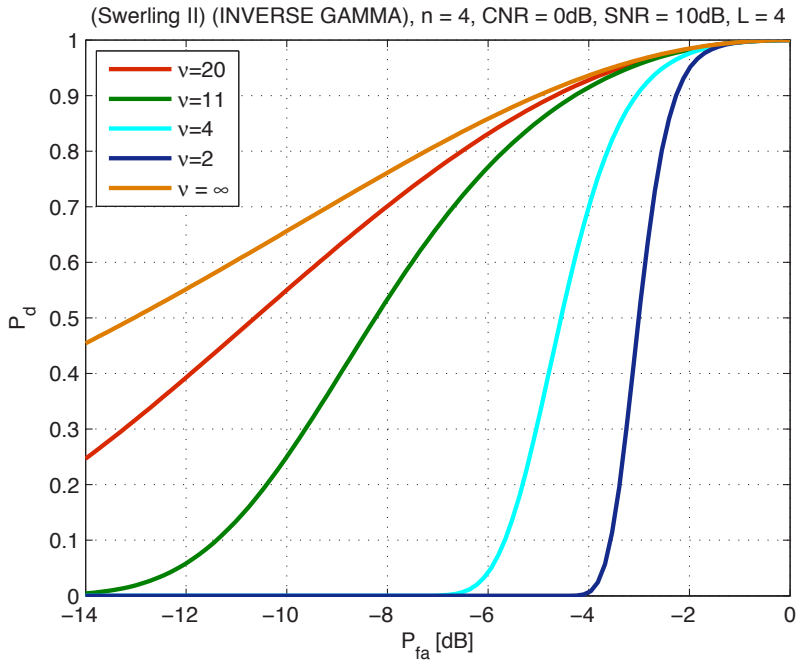

Figure 6: *P_{d} versus P_{fa} for the inverse Gamma texture and Swerling II target model with varying texture parameter ν.*

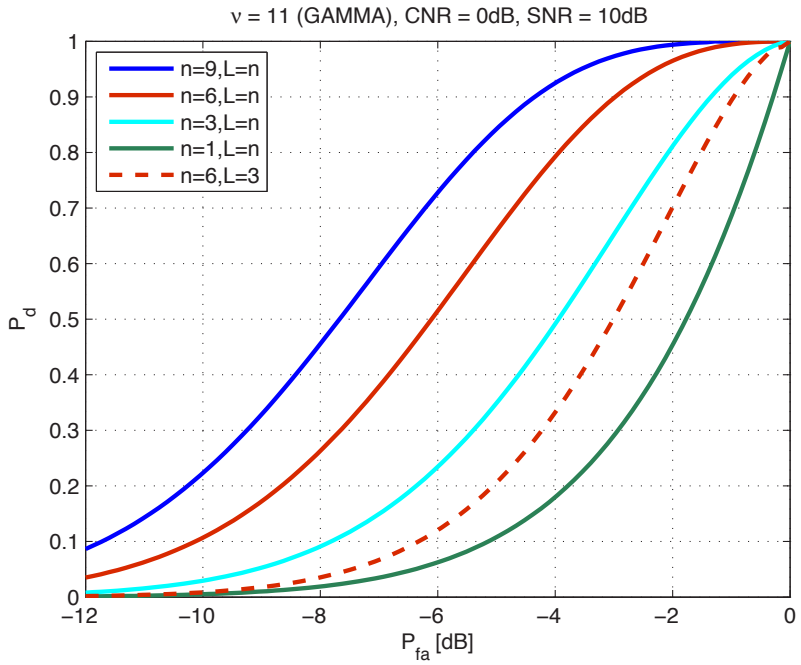

Figure 7: *P_{d} versus P_{fa} for the Gamma texture and Swerling II target model. Summation of channels was chosen with varying number of looks.*

7 Summary and conclusions

This memorandum presented several numerical approaches for computing the GMTI Receiver Operating Characteristics (ROC) of generic multi-channel radar systems. The development of the numerical approach permits the incorporation of a number of statistical models for the clutter, target and measurement system. The statistical models that have been considered are freely selectable and interchangeable and have sufficient breadth to cover a range of realistic scenarios. The utility and usefulness of the theoretical work has been demonstrated with examples featuring a variety of different parameter settings and processing methods.

The introduced tools have been successfully applied to study the performance of a potential GMTI mode on RCM [22].

References

[1] Ward, K. D., Tough, R. A. J., and Watts, S. (2006), Sea Clutter: Scattering, the K-distribution and Radar Performance, IET Radar, Sonar and Navigation, Series 20.

[2] Sikaneta, I. C. and Gierull, C. H. (2010), Adaptive CFAR for Space-Based Multi-Channel SAR-GMTI, In *Proc. 8th European Conference on SAR (EUSAR)*, pp. 1–4, Aachen, Germany.

[3] Gierull, C. H. (2004), Statistical Analysis of Multilook SAR Interferograms for CFAR Detection of Ground Moving Targets, *IEEE Trans. Geosci. Remote Sensing*, 42(4), 691–701.

[4] Cerutti-Maori, D., Gierull, C. H., and Ender, J. H. G. (2010), Experimental Verification of SAR-GMTI Improvement Through Antenna Switching, *IEEE Transactions on Geoscience and Remote Sensing*, 48(4), 2066–2075.

[5] Shnidman, D. A. (1995), Radar detection probabilities and their calculation, *IEEE Transactions on Aerospace and Electronic Systems*, 31(3), 928–950.

[6] Shnidman, D. A. (2003), Expanded Swerling target models, *IEEE Transactions on Aerospace and Electronic Systems*, 39(3), 1059–1069.

[7] Shnidman, D. A. (2005), Radar detection in clutter, *IEEE Transactions on Aerospace and Electronic Systems*, 41(3), 1056–1067.

[8] Shnidman, D. A. (2008), Update on radar detection probabilities and their calculation, *IEEE Transactions on Aerospace and Electronic Systems*, 44(1), 380–383.

[9] Conte, E. and Ricci, G. (1994), Performance prediction in compound-Gaussian clutter, *IEEE Transactions on Aerospace and Electronic Systems*, 30(2), 611–616.

[10] Gierull, C. H. (2002), Moving Target Detection with Along-Track SAR Interferometry - A Theoretical Analysis. DRDC Ottawa TR 2002-084, Defence Research and Development Canada.

[11] Swerling, P. (1997), Radar probability of detection for some additional fluctuating target cases, *IEEE Transactions on Aerospace and Electronic Systems*, 33(2), 698–709.

[12] Gierull, C. H. (2003), Digital Channel Balancing of Along-Track Interferometric SAR Data. DRDC Ottawa TM 2003-024, Defence Research and Development Canada.

[13] Frery, A. C., Müller, H.-J., Yanasse, C. F., and Sant'Anna, S. J. S. (1997), A Model for Extremely Heterogeneous Clutter, *IEEE Trans. Geoscience and Remote Sensing*, GRS-35(3), 648–659.

[14] Sikaneta, I. C. and Chouinard, J.-Y. (2004), Eigendecomposition of the multi-channel covariance matrix with applications to SAR-GMTI, *Signal Processing*, 84(9 (Special Issue)), 1501–1535.

[15] Bombrun, L. and Beaulieu, J.-M. (2008), Fisher Distribution for Texture Modeling of Polarimetric SAR Data, *IEEE Geoscience and Remote Sensing Letters*, 5(3), 512–516.

[16] Crisp, D. J., Rosenberg, L., Stacy, N. J., and Dong, Y. (2009), Modelling X-band sea clutter with the K-distribution: Shape parameter variation, In *Proc. RADAR Radar Conf. - Surveillance for a Safer World Int*, pp. 1–6.

[17] Joughin, I. R., Winebrenner, D. P., and Percival, D. B. (1994), Probability Density Functions for Multilook Polarimetric Signatures, *IEEE Trans. Geoscience and Remote Sensing*, GRS-32(3), 562–574.

[18] Roy, L. P. and Kumar, R. V. R. (2010), Accurate K-distributed clutter model for scanning radar application, *IET Radar, Sonar & Navigation*, 4(2), 158–167.

[19] Gierull, C. H. and Livingstone, C. (2004), SAR-GMTI Concept for RADARSAT-2, In Klemm, R., (Ed.), *The Applications of Space-Time Processing*, Stevenage, UK: IEE Press.

[20] Gradshteyn, I. S. and Ryzhik, I. M. (2000), Table of Integrals, Series and Products (Sixth Edition), 6 ed, Academic Press.

[21] Sikaneta, I. and Gierull, C. H. (2005), Two-Channel SAR Ground Moving Target Indication for Traffic Monitoring in Urban Terrain, In U. Stilla, U., Rottensteiner, F., and Hinz, S., (Eds.), *Proceedings of the ISPRS Workshop CMRT 2005, Object Extraction for 3D City Models, Road Databases and Traffic Monitoring - Concepts, Algorithms and Evaluation*, Vol. XXXVI, pp. 95–101, International Society for Photogrammetry and Remote Sensing, Vienna, Austria.

[22] Gierull, C. H. (2011), Potential SAR-GMTI capabilities of RCM/RNG. Oral Presentation at 2nd RADARSAT Next Generation Study User Group Meeting. DRDC Ottawa SL 2011-60.

Annex A: Special case of the conditional test pdf

This annex details the derivation of the conditional pdf in (26) in the absence of a target. The case $\boldsymbol{s} = \boldsymbol{0}$ implies $a = 0$ and hence leads to a division by zero. Using the relationship

$$I_{n-1}(2\sqrt{z}) = \frac{z^{\frac{n-1}{2}}}{\Gamma(n)}\, {}_0\mathrm{F}_1(n, z), \tag{A.1}$$

where ${}_0\mathrm{F}_1$ denotes the confluent hypergeometric function [20], (26) can be rewritten as

$$\begin{aligned} f_{T|\Delta}(t;\delta,a) &= \frac{(n\sigma^2)^{\frac{n+1}{2}}}{\Gamma(n)\overline{\sigma}^2}\left(\frac{t}{\cancel{a}}\right)^{\frac{n-1}{2}} \exp\left\{-\frac{n\sigma^2 t - a}{\overline{\sigma}^2}\right\}\left(\frac{n\sigma^2\cancel{a}t}{\overline{\sigma}^4}\right)^{\frac{n-1}{2}} {}_0\mathrm{F}_1\left(n, \frac{n\sigma^2 a}{\overline{\sigma}^4}t\right) \\ &= \left(\frac{n\sigma^2}{\overline{\sigma}^2}\right)^n \frac{t^{n-1}}{\Gamma(n)} \exp\left\{-\frac{n\sigma^2 t - a}{\overline{\sigma}^2}\right\} {}_0\mathrm{F}_1\left(n, \frac{n\sigma^2 a}{\overline{\sigma}^4}t\right). \end{aligned} \tag{A.2}$$

Using the property ${}_0\mathrm{F}_1(n, 0) = 1$, the conditional pdf in (26) for $a = 0$ becomes:

$$f_{T|\Delta}(t;\delta,0) = \left(\frac{n\sigma^2}{\overline{\sigma}^2}\right)^n \frac{t^{n-1}}{\Gamma(n)} \exp\left\{-\frac{n\sigma^2}{\overline{\sigma}^2}t\right\}. \tag{A.3}$$

This page intentionally left blank.

DOCUMENT CONTROL DATA

(Security classification of title, body of abstract and indexing annotation must be entered when document is classified)

1. ORIGINATOR (The name and address of the organization preparing the document. Organizations for whom the document was prepared, e.g. Centre sponsoring a contractor's report, or tasking agency, are entered in section 8.)

   Defence R&D Canada – Ottawa
   3701 Carling Avenue, Ottawa ON K1A 0Z4, Canada

2. SECURITY CLASSIFICATION (Overall security classification of the document including special warning terms if applicable.)

   UNCLASSIFIED
   (NON-CONTROLLED GOODS)
   DMC A
   REVIEW: GCEC June 2010

3. TITLE (The complete document title as indicated on the title page. Its classification should be indicated by the appropriate abbreviation (S, C or U) in parentheses after the title.)

   Numerical recipes to determine the performance of multi-channel GMTI radars

4. AUTHORS (Last name, followed by initials – ranks, titles, etc. not to be used.)

   Gierull, C. H.

5. DATE OF PUBLICATION (Month and year of publication of document.)	6a. NO. OF PAGES (Total containing information. Include Annexes, Appendices, etc.)	6b. NO. OF REFS (Total cited in document.)
December 2011	44	22

7. DESCRIPTIVE NOTES (The category of the document, e.g. technical report, technical note or memorandum. If appropriate, enter the type of report, e.g. interim, progress, summary, annual or final. Give the inclusive dates when a specific reporting period is covered.)

   Technical Memorandum

8. SPONSORING ACTIVITY (The name of the department project office or laboratory sponsoring the research and development – include address.)

   Defence R&D Canada – Ottawa
   3701 Carling Avenue, Ottawa ON K1A 0Z4, Canada

9a. PROJECT OR GRANT NO. (If appropriate, the applicable research and development project or grant number under which the document was written. Please specify whether project or grant.)	9b. CONTRACT NO. (If appropriate, the applicable number under which the document was written.)
15eq01	

10a. ORIGINATOR'S DOCUMENT NUMBER (The official document number by which the document is identified by the originating activity. This number must be unique to this document.)	10b. OTHER DOCUMENT NO(s). (Any other numbers which may be assigned this document either by the originator or by the sponsor.)
DRDC Ottawa TM 2011-230	

11. DOCUMENT AVAILABILITY (Any limitations on further dissemination of the document, other than those imposed by security classification.)

   (X) Unlimited distribution
   ( ) Defence departments and defence contractors; further distribution only as approved
   ( ) Defence departments and Canadian defence contractors; further distribution only as approved
   ( ) Government departments and agencies; further distribution only as approved
   ( ) Defence departments; further distribution only as approved
   ( ) Other (please specify):

12. DOCUMENT ANNOUNCEMENT (Any limitation to the bibliographic announcement of this document. This will normally correspond to the Document Availability (11). However, where further distribution (beyond the audience specified in (11)) is possible, a wider announcement audience may be selected.)

   Unlimited

13. ABSTRACT (A brief and factual summary of the document. It may also appear elsewhere in the body of the document itself. It is highly desirable that the abstract of classified documents be unclassified. Each paragraph of the abstract shall begin with an indication of the security classification of the information in the paragraph (unless the document itself is unclassified) represented as (S), (C), or (U). It is not necessary to include here abstracts in both official languages unless the text is bilingual.)

This memorandum presents a robust and relatively simple-to-implement numerical approach for computing figures of merits, such as probability of detection and probability of false alarms. Figures of merit can be computed to a chosen arbitrary accuracy for generic Ground Moving Target Indicator (GMTI) radars under specified general assumptions for the interfering clutter and desired target signal statistics. The approach expands the well-published single receiver channel analysis to multi-channel approaches, such as the Displaced Phase Center Antenna DPCA or Space-Time Adaptive Processing (STAP) without relying on a common approximation for non-homogeneous clutter (texturizing the noise) to make the models mathematically tractable. The derivation comprises a flexible modeling approach permitting solutions for a variety of target models including deterministic targets and the fluctuating target Radar Cross Section (RCS) Swerling target models. The approach additionally allows for the averaging of multiple independent measurements (multi-looking). The capability and usefulness of this new approach is demonstrated based on numerical examples with a variety of different radar parameter settings.

14. KEYWORDS, DESCRIPTORS or IDENTIFIERS (Technically meaningful terms or short phrases that characterize a document and could be helpful in cataloguing the document. They should be selected so that no security classification is required. Identifiers, such as equipment model designation, trade name, military project code name, geographic location may also be included. If possible keywords should be selected from a published thesaurus. e.g. Thesaurus of Engineering and Scientific Terms (TEST) and that thesaurus identified. If it is not possible to select indexing terms which are Unclassified, the classification of each should be indicated as with the title.)

Synthetic Aperture Radar; Ground Moving Target Detection; RADARSAT Constellation Mission; Probability of False Alarms; Probability of Detection

Defence R&D Canada

Canada's leader in Defence
and National Security
Science and Technology

R & D pour la défense Canada

Chef de file au Canada en matière
de science et de technologie pour
la défense et la sécurité nationale

www.drdc-rddc.gc.ca